Published in final edited form as:
Proteins. 2010 February 15; 78(3): 661–670. doi:10.1002/prot.22595.

Nitric Oxide Conduction by the Brain Aquaporin AQP4

Yi Wang and **Emad Tajkhorshid***
Center for Biophysics and Computational Biology, Department of Biochemistry, and Beckman Institute for Advanced Science and Technology, University of Illinois at Urbana-Champaign, Urbana, IL, 61801, USA

Abstract

Involvement of aquaporins in gas conduction across the membrane and the physiological significance of this process have attracted marked attention from both experimental and theoretical studies. Previous work demonstrated that AQP1 is permeable to both CO_2 and O_2. Here we employ various simulation techniques to examine the permeability of the brain aquaporin AQP4 to NO and O_2 and to describe energetics and pathways associated with these phenomena. The energy barrier to NO and O_2 permeation through AQP4 central pore is found to be only ~3 kcal/mol. The results suggest that the central pore of AQP4, similar to that of AQP1, can indeed conduct gas molecules. Interestingly, despite a longer and narrower central pore, AQP4 appears to provide an energetically more favorable permeation pathway for gas molecules than AQP1, mainly due to the different orientation of its charged residues near the pore entrance. Although the low barrier against gas permeation through AQP4 indicates that it can participate in gas conduction across the cellular membrane, physiological relevance of the phenomenon remains to be established experimentally, particularly since pure lipid bilayers appear to present a more favorable pathway for gas conduction across the membrane. With an energy well of −1.8 kcal/mol, the central pore of AQP4 may also act as a reservoir for NO molecules to accumulate in the membrane.

Introduction

Aquaporins (AQPs) are a family of membrane channels (1) that, through modulating the water permeability of biological membranes, play a significant role in water homeostasis in living cells (2,3). Since their discovery by Agre and coworkers (1), significant effort has been put into structural characterization of these channels. As a result, AQPs now represent the richest family of membrane channels with regard to the abundance of high resolution structural data. Three-dimensional structures at atomic resolution are available for *E. coli* GlpF (4,5) and AqpZ (6), human AQP1 (7), bovine AQP1 (8), archaeal AqpM (9), rat AQP4 (10), as well as bovine and sheep AQP0 at two different pH conditions (11,12). The structure of human AQP2 has also been solved with a resolution of 4.5 Å (13). Most recently, two new AQP structures have been reported, namely, the structures of a plant AQP (spinach PIP2) in both the closed and open states (14), and the structure of human AQP5 (15).

The availability of high resolution structures and the timescale associated with their primary biological function, *i.e.*, water conduction, have made AQPs an ideal system for molecular dynamics (MD) simulations. In particular, an intriguing property of AQPs, namely, the ability to block protons while allowing rapid water conduction, has been the subject of extensive theoretical studies (5,16–18). As these studies unravel the mechanism of proton exclusion in AQPs, further structural and functional analyses begin to reveal that AQPs may

*To whom correspondence should be addressed. Phone: (217) 244-6914, emad@life.uiuc.edu.

be more than just simple, always-open water channels. For instance, while most AQPs are believed to operate as permanently open channels, gating of water pores has been demonstrated for a large number of them, particularly for, but not limited to, plant AQPs (19). Gating is found to be controlled either by phosphorylation of highly conserved serine residues, or, by variations in the intracellular pH. The phosphorylation-mediated gating of spinach aquaporin SoPIP2;1 has been recently investigated in a combined experimental and theoretical study (14,20).

In addition to water conduction, involvement of AQPs in conduction of other small molecules, such as glycerol (21,22), urea (23), nitrate (24), arsenite (25) and even ions (26,27) has been reported. AQPs have also been extensively studied for their participation in gas conduction across cellular membranes (28–40). For instance, human AQP1, when reconstituted in proteoliposomes, has been found to increase both water and CO_2 permeabilities markedly (31), and the tobacco aquaporin NtAQP1 is shown to play a role in photosynthesis and stomatal opening by facilitating CO_2 transport across the membrane (28). However, evidence against a physiological role of AQP-mediated gas conduction has also been reported (41–43). The controversy appears to be due to technical difficulties associated with accurate measurement of gas permeation across biological membranes, as well as the lipid composition differences between whole cell/tissue systems (whose lipid composition is often unknown) and the artificial membranes employed to measure gas permeability in these studies. In particular, the gas permeation through proteins is often masked by the high gas permeability of the employed artificial lipid bilayer; in other words, it becomes very difficult to identify whether gas molecules are also conducted by the proteins embedded in the membrane. MD simulations, which provide atomic details of the system under investigation, thus, become an important tool in characterizing the permeability of AQPs to gas molecules. Two recent MD studies (44,45) have investigated conduction of various gas species, CO_2 and O_2, through mammalian AQP1 and characterized the energetics associated with permeation of these gas species through the water pores and the central pore of AQP1. Both reports find that the artificial lipid bilayers used for the simulations presented an energetically more favorable pathway for gas conduction, but emphasize the fact that the free energy barrier against gas permeation through AQPs is easily surmountable by gas molecules at room temperature, concluding that AQP-mediated gas conduction may be physiologically relevant in membranes with low intrinsic gas permeability (yet to be demonstrated *in vivo*, experimentally), or when AQPs constitute a significant portion of the membrane surface area. In this work, we extend the scope of these studies and investigate gas permeation through the mammalian CNS aquaporin AQP4 and the associated pathways and energetics. While appearing structurally similar, AQPs show surprisingly distinct properties within the family with regard to their substrate selectivity. Therefore, it is relevant to examine permeability of AQP4, which is an abundant AQP in the brain and which might exhibit particular features with regard to gas permeation, especially with respect to NO, which is an important neurotransmitter and signaling molecule. We note that the central pore of AQP4 is longer and narrower at certain regions when compared to AQP1, and one might expect it to be a less efficient conduit for gas molecules. As will be described later in the present paper, this turns out not to be the case, and in fact AQP4 is found to provide an energetically more favorable conduction pathway for gas molecules than AQP1.

AQP4 is the predominant water channel in the central nervous system (CNS), where it is most abundant in astroglial cells that surround capillaries and form glia limitans, as well as in ependymal cells lining ventricles (46,47). AQP4 plays an important role in cerebral water balance under normal and pathological conditions (48,49). Moreover, its indirect role in neuronal signal transduction has also been suspected (48). An interesting feature of AQP4, revealed experimentally by freeze fracture and immunogold methods, is the formation of

extensive 2D square arrays in the membrane of astrocyte endfeet and ependymal cells (10,50–52). In these cells, large sets of tightly packed AQP4 occupy a significant portion of certain areas of the cell membrane. This property of AQP4 as well as its importance as the predominant water channel in the brain inspired us to examine its gas permeability, in particular for NO and O_2.

Since its early description as the endothelium-derived relaxing factor (EDRF), NO has been found to be a fundamental messenger that modulates blood flow, thrombosis, and neural activity in all vertebrates (53–55). In peripheral organs, NO triggers the relaxation of vascular smooth muscles, thereby increasing the blood flow (53–55); In the CNS, NO acts as a neurotransmitter and plays a role in various physiological processes, *e.g.*, sleep, learning and memory (56). Recently, it has been suggested that AQP1 can mediate the permeation of NO across endothelial membranes, and play a role in NO-dependent vasorelaxation (37,40). In the present study, we employ several complementary simulation techniques to investigate the permeability of AQP4 to NO and O_2. Following our preliminary work (57), we provide comprehensive evidence that AQP4 is permeable to both NO and O_2, characterize the conduction pathways in AQP4, and present a comparison of its gas permeability with AQP1.

Methods

Modeling

We build the simulation system of an AQP4 tetramer as follows: A 120×120 $Å^2$ POPE bilayer patch is first built using VMD's membrane plugin (58), with the membrane normal along the *z*-axis (Fig. 1). A tetramer of AQP4 (pdb code 2d57 (10)) is embedded in this bilayer and lipid molecules within 0.8 Å of heavy atoms of the protein are removed. Two 18-Å slabs of water are then added using the solvate plugin of VMD (58) to fully hydrate the bilayer. To neutralize the system, 23 Na^+ and 19 Cl^- ions are added using VMD's autoionize plugin (58), generating a 100 mM ionic concentration. This system is first minimized for 5,000 steps, then the lipid tails are "melted" in a 500-ps constant temperature (310 K) and constant volume (NVT) simulation in which only the lipid tails are free to move. Another 500-ps simulation is performed under constant temperature (310 K) and constant pressure (1 atm) conditions (NPT), with the C_α atoms of the protein constrained using harmonic potentials (k = 7.2 kcal/mol/$Å^2$). After releasing the constraints, the system is further simulated under the same NPT conditions for another 2.5 ns. To distinguish the system from the one used in explicit gas diffusion simulations, we refer to this system as *apo*-AQP4.

Explicit gas diffusion simulation

Starting with the *apo*-AQP4 system described above, we build the system for explicit gas diffusion simulation by replacing 150 water molecules with NO. As shown in Fig. 1, these NO molecules are initially placed in the bulk solvent, at least 5 Å away from the protein. The system is then minimized for 5,000 steps and simulated under NVT (T=300 K) conditions for 50 ns.

Implicit ligand sampling

In order to perform implicit ligand sampling, the *apo*-AQP4 system is further simulated under NVT (T=300 K) conditions for 10 ns. The last 9 ns of this simulation is used for the implicit ligand sampling calculations. The implicit ligand sampling is a method to compute the potential of mean force (PMF) of a weakly interacting ligand from an equilibrium simulation of the ligand-free system (59,60). The method has been applied to study the O_2 permeability of AQP1 in our previous study (44). By placing an NO or O_2 molecule at every

grid point (1 Å apart) in the *apo*-AQP4 system, a 3D PMF map of the gas molecule is calculated (59,60):

$$F(x,y,z) = -RT\ln\frac{\left\langle \int d\Omega e^{-\Delta E(x,y,z,\Omega)/RT} \right\rangle}{\int d\Omega} \quad (1)$$

where ΔE is the interaction energy between the gas molecule and the *apo*-AQP4 system, Ω represents the orientational degrees of freedom of NO or O_2, and ⟨…⟩ denotes an ensemble average. The 3D PMF is then used to obtain the PMF along a selected reaction coordinate, *e.g.*, the channel axis of the AQP4 central pore:

$$F(z) = -RT\ln\sum_{x,y=0}^{L_x,L_y}\frac{e^{-F(x,y,z)/RT}}{L_xL_y} \quad (2)$$

where L_x and L_y are dimensions of the area where the summation is performed, *e.g.*, the cross-section of AQP4 central pore. In the bulk water region, the summation is performed in a square centered at the central pore, with an area roughly equal to the area occupied by an AQP4 tetramer (50 nm^2). Thus, the resulting PMF can account for the entropy loss of a gas molecule when it enters an AQP4 tetramer from the bulk water, and can be directly compared with the PMF of a lipid bilayer.

It is worth mentioning that the PMFs calculated above has vacuum as their reference point, *i.e.*, the PMF is zero when the gas molecule is in vacuum. This is slightly different from the convention used by many other free energy calculations, where PMF is often set to zero when the ligand is in bulk water. In our calculations, the PMF in bulk water corresponds to the solvation energy of the gas molecules, and can be compared directly with experimental measurements. For this reason, we keep the reference of the PMFs to vacuum. The PMFs obtained from umbrella sampling (see below), which initially have their reference set to bulk water, are shifted by the solvation energy of the corresponding gas species, in order to provide a better comparison with the implicit ligand sampling results.

Umbrella sampling

Umbrella sampling is used to calculate the PMF of NO permeation through the AQP4 central pore. We start with the final structure of the 10-ns *apo*-AQP4 simulation prepared for implicit ligand sampling, and divide the central axis of AQP4 into 1.0-Å segments (windows). Umbrella sampling is performed by restraining an NO molecule to the center of each window using a harmonic potential with a force constant of 8.63 kcal/mol/$Å^2$. Note that the restraint is applied to the center-of-mass of the NO molecule and only along the channel axis (*z*-axis). To reduce the computational cost, two windows are sampled simultaneously in each simulation. Similar to a previous study (45), the two windows are separated by at least 25 Å, so that the interaction between the two NO molecules is negligible. A 2-ns simulation is performed for each window, with the first 0.4 ns considered equilibration and the remaining 1.6 ns used to construct the PMF using the weighted histogram analysis method (WHAM) (61). Since a complete sampling of the bulk water region cannot be achieved within the employed simulation timescale, we restrict the sampling of the bulk water to a cylinder centered at the geometric center of the AQP4 tetramer with a radius R=10 Å. The PMF of this region is then shifted by $-RT\ln(\pi R^2/A_0)$, where A_0 (50 nm^2) is the area of an AQP4 tetramer. The shift accounts for the entropy difference between the sampled area and a bulk water region of the same area as an AQP4

tetramter. The resulting PMF can then be compared directly with that obtained from the implicit ligand sampling simulation, as well as with that of a pure lipid bilayer. Collectively, 66 ns of simulations are performed for umbrella sampling.

PMF of water permeation

The PMF of water permeation is calculated using the 10 ns *apo*-AQP4 simulation prepared for implicit ligand sampling. Average water occupancy is obtained using VMD's volmap plugin (60), and the PMF of water permeation through the four monomeric water pores is then constructed using an equation similar to Eq. 2, with the local water occupancy $P(x,y,z)$ replacing $e^{-F(x,y,z)/RT}$.

Simulation protocols

For all MD simulations, the program NAMD 2.6 (62) and the CHARMM27 parameter set (63) are used. Langevin dynamics is used to keep the temperature constant (300 K, unless specified otherwise) with a damping coefficient of 5 ps^{-1}. During the umbrella sampling simulations, the damping coefficient is set to 0.1 ps^{-1}. For NPT simulations, a Langevin piston (64) is employed to maintain the pressure at 1 atm. Assuming periodic boundary conditions, the particle mesh Ewald (PME) method (65) with a grid density of at least $1/Å^3$ is employed for computation of long-range electrostatic forces. All simulations are performed with time steps of 1, 2, and 4 fs for calculation of bonded, non-bonded, and PME interactions, respectively. Parameters for NO and O_2 are the same as used in a previous study (60), which have been shown to reproduce the solvation energy of these gas molecules. The small partial charges of NO ($q_N = 0.025e$, $q_O = -0.025e$) are found to have a negligible effect on its solvation energy (60), allowing us to use a charge-less model of NO, and, thus, avoid the expensive electrostatic interaction calculations in implicit ligand sampling. In all the simulations, including the implicit ligand sampling ones, both the oxygen atoms in O_2 are neutral, i.e., they do not carry any partial charges.

Results and Discussion

AQP4 is permeable to NO and O_2

To investigate the permeability of AQP4 to NO, we used three complementary methods, namely, explicit gas diffusion simulation, implicit ligand sampling, and umbrella sampling. In the explicit gas diffusion simulation, we start with 150 NO molecules randomly placed in the bulk water on both sides of a membrane-embedded AQP4 tetramer (Fig. 1). As the simulation proceeds, NO molecules begin to diffuse and encounter the AQP4 tetramer as well as the lipid bilayer. Their fairly rapid partition between water and the protein reflects the ease of NO entrance into the AQP4 channel, thus providing a first indication of the gas permeability of AQP4. This simulation also allows us to directly analyze the interaction between gas molecules and the protein. The implicit ligand sampling and umbrella sampling are then used to produce a quantitative description, *i.e.*, the free energy profile (PMF), of NO permeation through AQP4. Using implicit ligand sampling, we also calculated the PMF of O_2 permeation through AQP4. Below we present the results of these simulations in detail.

As shown in Fig. 2a, two quadruplets of hydrophobic residues, Leu66 and Leu191, form the outermost gates of the AQP4 central pore. Water molecules can hardly cross these gates and are, thus, kept out of the central pore throughout the simulation. In contrast, seven NO molecules are found to enter the central pore of AQP4 spontaneously during the 50-ns explicit gas diffusion simulation. Due to the short time scale of the simulation, no complete permeation events were observed. However, given the readiness of NO crossing the periplasmic and cytoplasmic gates of the central pore, it is reasonable to assume that complete permeation events will occur on longer time scales. Indeed, PMF of NO

permeation calculated using implicit ligand sampling revealed an energy well of −1.8 kcal/mol in the middle of the central pore, and an energy barrier of only ~2.9 kcal/mol at the two entrances (Fig. 3). A slightly higher barrier (3.3 kcal/mol) is obtained using umbrella sampling. To put these energy barriers in the context, we have also calculated the PMF of water permeation through the four monomeric water pores. The calculation reveals a 3.0 kcal/mol energy barrier for water (Supplementary Fig. S1), which is comparable with the reported value from a previous simulation for AQP1 (45). Clearly, the energy barrier of NO permeation through the central pore is similar to that of water permeation through the water pores. Therefore, from an energetic point of view, the central pore can conduct gas molecules as readily as water pores conduct water.

Using implicit ligand sampling, we have also calculated the PMF of O_2 permeation. As shown in Fig. 3c, a 2.9 kcal/mol energy barrier is revealed, which is similar to that of NO. These numbers indicate that the central pore of AQP4 is permeable to both gas species. This permeability is explained by the hydrophobic composition of the central pore: the interior of the central pore in AQP4 ($-7 \leq z \leq 20$, with the center of the protein at $z = 0$) is composed entirely of hydrophobic residues, which impose a significant energy barrier against water permeation. In contrast, nonpolar gas molecules can readily enter such a hydrophobic environment and use it as a pathway to cross the membrane. The energy barrier to this process appears to be mainly entropic in nature. As shown in Fig. 3b, the loss of NO-water interactions (ΔE_{wat}) is largely compensated by the gained NO-protein interactions (ΔE_{pro}), resulting in only a small change in total enthalpy (ΔE_{tot}).

Unlike the central pore, the monomeric pores of AQP4, which are empty at the beginning of the simulation, become hydrated almost immediately (within 0.5 ns). Water molecules form a single file inside each monomeric pore, adopting a characteristic bipolar orientation, which has been observed in all AQP simulations (5,66,67). NO molecules are found to enter the water pores occasionally during the 50-ns explicit gas diffusion simulation, as shown in Fig. 2b. However, in contrast to the central pore, where gas molecules freely visit the entire pore, no gas molecule is found at the selectivity filter (SF), *i.e.*, the narrowest part of the water pores. Using implicit ligand sampling, we measured the energy barriers of NO and O_2 permeation through the water pore as 5.8 kcal/mol and 4.9 kcal/mol, respectively (Fig. 3). The highest barrier is located at the SF ($z = 5$ Å), consistent with the results of the explicit gas diffusion simulation. As also reported in previous studies (44,45,68), these energy barriers are caused by the disruption of the hydrogen bond network of water molecules inside the water pores due to insertion of gas molecules. Since the central pore is not pre-occupied with water, it provides a more favorable pathway for NO and O_2 in comparison to the water pores. With this regard, it is worth mentioning that a lipid molecule was reported to occupy the central pore of AQP5 in a recent crystal structure (15). Naturally, occupancy of the central pore by such a large molecule as a lipid will have significant ramifications on its gas permeability. However, we note that a lipid-filled central pore might represent a unique feature for AQP5, since no other AQP structure reported to date, including the structure AQP4 (10) which is the subject of the present study, includes a lipid molecule in its central pore.

AQP4 conducts gas molecules better than AQP1

Our previous study revealed a 3.6–4.6 kcal/mol energy barrier against O_2 permeation through the central pore of AQP1, and a 5.7 kcal/mol barrier against permeation through its water pores (44). In comparison, energy barriers of 2.9 kcal/mol and 4.9 kcal/mol are found for O_2 permeation through AQP4 central pore and water pores, respectively. Thus, AQP4 appears to conduct gas molecules more readily than AQP1. This result may seem surprising, since the central pores of the two AQPs might appear to be very similar at the first glance. A close examination of the crystal structures, however, reveals that AQP4 has a much

narrower and longer central pore than that of AQP1. As shown in Fig. 4a, the transmembrane helix H2 in AQP4 extends an extra turn. Residue Leu66 from this turn almost completely blocks the periplasmic entrance of the central pore (Fig. 4b). As a result, one may expect the central pore of AQP4 to impose a higher energy barrier to gas permeation than AQP1. Interestingly, it turns out that the central pore of AQP4 provides a better gas conduction pathway than that of AQP1.

Analysis of our explicit gas diffusion simulation shows that due to the thermal fluctuations of residues at its periplasmic entrance, the AQP4 central pore can undergo a significant "breathing" motion. The four-fold symmetry observed in the crystal structure is broken during this process, and transient pathways open for NO molecules, allowing them to freely cross the periplasmic gate. Two representative NO pathways revealed by the explicit gas diffusion simulation are shown in Figs. 5a and 5b. Note that apart from a "straight" pathway which is parallel to the channel axis of the central pore (Fig. 5a), there also exist "tilted" pathways that run below Leu66 (Fig. 5b). These pathways, which are also revealed by implicit ligand sampling (Fig. 5c), provide additional routes for NO to enter the central pore, thereby, significantly lowering the energy barrier against its permeation. It is noteworthy that water molecules hardly enter these pathways, consistent with the mostly hydrophobic nature of these pathways. The AQP4 central pore therefore offers an exclusive pathway for gas molecules.

In AQP1, four Asp50 residues form a ring at the periplasmic entrance of the central pore, each pointing its side chain towards the pore (Fig. 4c). We have shown that these charged residues anchor a dense layer of water molecules near the pore entrance (44). With a higher density and less fluctuation than bulk water, this water layer was suggested to reduce the chance of gas molecules to enter and cross the central pore (44). When Asp50 was mutated to a neutral residue, e.g., alanine or asparagine, the strong electrostatic effects of the quadruplet vanished and a significantly smaller energy barrier in this region was revealed (data not shown). In AQP4, residue Asp69 is in a similar position to Asp50 in AQP1. Unlike Asp50, however, the four Asp69 residues point their side chains away from the central pore (Fig. 4d). This seemingly small conformational variation has a dramatic effect: while the periplasmic entrance of AQP1 central pore is covered by a dense layer of water molecules, the entrance of AQP4 central pore is rather "clear" (Fig. 4d). Consequently, gas molecules entering the AQP4 central pore are not hindered by unfavorable interactions with water. This effect helps lower the energy barrier to gas permeation. The barrier might be further lowered by mutating the gate residues Leu66 and Leu191 to alanines, since the smaller alanine residues introduce more free volume in the barrier regions while maintaining the hydrophobicity of the channel.

Physiological relevance of AQP4-mediated gas permeation

While extensive experimental (28,34–36,40) and theoretical (44,45,68) studies have established that AQPs can conduct gas molecules, the physiological relevance of AQP-mediated gas conduction remains a matter of debate (38–40). Although our simulation results provide strong support for gas conduction through these *porous* proteins (AQP1 and AQP4), the physiological relevance of the observed phenomenon is beyond the scope of the present study and remains to be established experimentally. On this subject, recent studies (38,39) offer different views: Endeward, *et. al* suggested that AQP1 is a major pathway for CO_2 transport across the human erythrocyte membrane (36). Uehlein, *et. al* showed that the plant aquaporin NtAQP1 contributes significantly to CO_2 permeability of chloroplast membranes (38). On the other hand, Missner, *et. al* reported that the resistance to transmembrane CO_2 permeation is mainly caused by the unstirred layer (USL), and not the membrane itself, thereby, suggesting that facilitation of CO_2 transport by membrane proteins is not physiologically important (39).

Previous simulations both from our laboratory and from others have shown that although AQP1 is permeable to both CO_2 and O_2, pure phospholipids bilayers, *e.g.*, POPE, present a much lower energy barrier against the permeation of these gas molecules (44,45). In the present study, we applied implicit ligand sampling on a larger patch of POPE bilayer and calculated its NO and O_2 permeability. As shown in Fig. 3d, the energy barriers to NO and O_2 permeation are found to be 0.3 kcal/mol and 0.4 kcal/mol, respectively. These numbers are essentially negligible when compared with the energy barrier calculated for gas permeation through AQP4. Therefore, if the cellular membrane exhibits a similar degree of gas permeability to that of the artificial lipid bilayers (e.g., POPE) used in simulation studies, APQs are not expected to play a significant role in gas exchange across the membrane. In other words, AQP-mediated gas conduction can only be physiologically relevant in membranes with low intrinsic gas permeability, or when AQPs occupy a large portion of the membrane surface. It is noteworthy that the latter case seems to be relevant to AQP4. In the CNS, AQP4 has a highly polarized distribution, with greatest abundance in astrocyte endfeet that surround capillaries and form the glia limitans, as well as in ependymal cells (46,47,69). As revealed by freeze fracture and immunogold studies (50–52), AQP4 arrays in astrocytes and ependymal cells can occupy a significant portion of the membrane in certain areas. In these areas, the membrane is essentially a “proteinaceous” membrane rather than a lipid membrane. Hence, it is of particular interest to examine the physiological significance of the AQP4-mediated gas conduction in these cells.

In the CNS, NO is mainly produced by two isoforms of NO synthase (NOS), neuronal NOS (nNOS) and endothelial NOS (eNOS) (70). While nNOS is found in neurons and has a wide distribution in the brain, eNOS is primarily located in endothelial cells (70). Interestingly, AQP4 may be found in the proximity of both nNOS and eNOS: AQP4 exists in the plasma membranes of astrocytes, which are glial cells surrounding neurons. More importantly, the endfeet of astrocytes, which have a high density of AQP4 arrays, are known to surround endothelial cells of capillaries. In addition, the presence of eNOS in astrocytes has also been suspected (71). Recent experimental studies on AQP1 suggest that it mediates NO permeation both when reconstituted in lipid vesicles (37) and *in vivo* (40). In the present study, we have demonstrated that compared with AQP1, AQP4 is more adapted for gas conduction. Together with the fact that AQP4 forms high-density arrays in cells near NO sources, it would be of interest to investigate as to whether AQP4 might play a role in the control of NO flow in the CNS. In addition, as the central pore of AQP4 has an energy well comparable to that found in a lipid bilayer, it might also serve as an additional reservoir for NO molecules in the membrane.

Conclusions

The participation of AQPs in gas conduction across cellular membranes has been a subject that attracted significant attention from both theoreticians and experimentalists (28–37). Two questions appear to be central to this subject: (1) whether AQPs can conduct gas molecules, i.e., whether there are conduction pathways in the protein that allow permeation of gas species, and (2) whether AQP-mediated gas conduction is of physiological relevance, the answer to which is beyond the scope of the present study and relies on experimental studies. Continuing our previous work on AQP1 (44), we sought to address question (1) by studying the permeability of AQP4 to NO and O_2 using MD simulations of membrane-embedded AQP4 tetramer and pure lipid bilayers. Three different approaches, namely, explicit gas diffusion simulation, implicit ligand sampling, and umbrella sampling, were employed to characterize gas permeation through AQP4. These methods yielded consistent results, demonstrating that AQP4 presents a low energy barrier against NO and O_2 permeation, thus, providing a direct answer to question (1). The central pore of AQP4 is found to be more conductive of gas species than the monomeric water pores. Moreover,

despite the longer and narrower central pore, AQP4 serves as a better gas conduit than AQP1.

Compared with the free energy profile of gas permeation through AQPs, an artificial phospholipid bilayer, e.g., POPE, is found to have a much lower energy barrier. Therefore, assuming a comparable level gas of permeability for a real cellular membrane, lipid bilayers appear to provide the main pathway for gas conduction into and out of a cell, and gas conduction through AQPs can only be of physiological importance either in membranes with low intrinsic gas permeability or when a major fraction of the surface area of the membrane is occupied by AQPs. Recent experiments (37) have demonstrated that AQP1 can conduct NO when over-expressed in CHO-K1 cells and when reconstituted into lipid vesicles. Similar experimental studies are required to elucidate the role of AQP4-mediated gas conduction in vitro and in the CNS.

Supplementary Material

Refer to Web version on PubMed Central for supplementary material.

Acknowledgments

This work was supported by grants from NIH (R01-GM067887 and P41-RR05969). The authors gladly acknowledge computer time provided by the Large Resource Allocation Committee (MCA06N060), as well as computer time from the DoD High Performance Computing Modernization Program at the Arctic Region Supercomputing Center, University of Alaska at Fairbanks. The authors would also like to acknowledge Dr. Jordi Cohen for his help on the implicit ligand sampling method.

References

1. Preston GM, Carroll TP, Guggino WB, Agre P. Appearance of water channels in Xenopus oocytes expressing red cell CHIP28 protein. Science. 1992; 256:385–387. [PubMed: 1373524]
2. Agre P, Kozono D. Aquaporin water channels: molecular mechanisms for human diseases. FEBS Lett. 2003; 555:72–78. [PubMed: 14630322]
3. King L, Agre P. From structure to disease: The evolving tale of aquaporin biology. Nat Rev Mol Cell Biol. 2004; 5:687–698. [PubMed: 15340377]
4. Fu D, et al. Structure of a glycerol conducting channel and the basis for its selectivity. Science. 2000; 290:481–486. [PubMed: 11039922]
5. Tajkhorshid E, et al. Control of the selectivity of the aquaporin water channel family by global orientational tuning. Science. 2002; 296:525–530. [PubMed: 11964478]
6. Savage DF, Egea PF, Robles-Colmenares Y, O'Connell JD III, Stroud RM. Architecture and selectivity in aquaporins: 2.5 Å X-ray structure of aquaporin Z. PLoS Biology. 2003; 1:E72. [PubMed: 14691544]
7. Murata K, et al. Structural determinants of water permeation through aquaporin-1. Nature. 2000; 407:599–605. [PubMed: 11034202]
8. Sui H, Han BG, Lee JK, Walian P, Jap BK. Structural basis of water-specific transport through the AQP1 water channel. Nature. 2001; 414:872–878. [PubMed: 11780053]
9. Lee JK, et al. Structural basis for conductance by the archaeal aquaporin AqpM at 1.68 Å. Proc Natl Acad Sci USA. 2005; 102:18932–18937. [PubMed: 16361443]
10. Hiroaki Y, et al. Implications of the Aquaporin-4 structure on array formation and cell adhesion. J Mol Biol. 2006; 355:628–639. [PubMed: 16325200]
11. Gonen T, Sliz P, Kistler J, Cheng Y, Walz T. Aquaporin-0 membrane junctions reveal the structure of a closed water pore. Nature. 2004; 429:193–197. [PubMed: 15141214]
12. Harries WEC, Akhavan D, Miercke LJW, Khademi S, Stroud R. The channel architecture of aquaporin 0 at a 2.2-angstrom resolution. Proc Natl Acad Sci USA. 2004; 101:14045–14050. [PubMed: 15377788]

13. Scheuring S, Busselez J, Lévy D. Structure of the dimeric PufX-containing core complex of *Rhodobacter blasticus* by *in situ* atomic force microscopy. J Biol Chem. 2005; 280:1426–1431. [PubMed: 15522874]
14. Törnroth-Horsefield S, et al. Structural mechanism of plant aquaporin gating. Nature. 2006; 439:688–694. [PubMed: 16340961]
15. Horsefield R, et al. High-resolution X-ray structure of human aquaporin 5. Proc Natl Acad Sci USA. 2008; 105:13327–13332. [PubMed: 18768791]
16. Burykin A, Warshel A. On the origin of the electrostatic barrier for proton transport in aquaporin. FEBS Lett. 2004; 570:41–46. [PubMed: 15251436]
17. de Groot BL, Grubmüller H. Water permeation across biological membranes: Mechanism and dynamics of aquaporin-1 and GlpF. Science. 2001; 294:2353–2357. [PubMed: 11743202]
18. de Groot BL, Grubmüller H. The dynamics and energetics of water permeation and proton exclusion in aquaporins. Curr Opin Struct Biol. 2005; 15:176–183. [PubMed: 15837176]
19. Hedfalk K, et al. Aquaporin gating. Curr Opin Struct Biol. 2006; 16:447–456. [PubMed: 16837191]
20. Nyblom M, et al. Structural and functional analysis of SoPIP2;1 mutants add insight into plant aquaporin gating. J Mol Biol. 2009; 387:653–668. [PubMed: 19302796]
21. Heller KB, Lin EC, Wilson TH. Substrate specificity and transport properties of the glycerol facilitator of *Escherichia coli*. J Bacteriol. 1980; 144:274–278. [PubMed: 6998951]
22. Borgnia MJ, Agre P. Reconstitution and functional comparison of purified GlpF and AqpZ, the glycerol and water channels from *Escherichia coli*. Proc Natl Acad Sci USA. 2001; 98:2888–2893. [PubMed: 11226336]
23. Borgnia M, Nielsen S, Engel A, Agre P. Cellular and molecular biology of the aquaporin water channels. Annu Rev Biochem. 1999; 68:425–458. [PubMed: 10872456]
24. Ikeda M, et al. Characterization of aquaporin-6 as a nitrate channel in mammalian cells. Requirement of pore-lining residue threonine 63. J Biol Chem. 2002; 277:39873–39879. [PubMed: 12177001]
25. Liu Z, et al. Arsenite transport by mammalian aquaglyceroporins AQP7 and AQP9. Proc Natl Acad Sci USA. 2002; 99:6053–6058. [PubMed: 11972053]
26. Yool AJ, Weinstein AM. New roles for old holes: Ion channel function in aquaporin-1. News Physio Sci. 2002; 17:68–72.
27. Yu J, Yool AJ, Schulten K, Tajkhorshid E. Mechanism of gating and ion conductivity of a possible tetrameric pore in Aquaporin-1. Structure. 2006; 14:1411–1423. [PubMed: 16962972]
28. Uehlein N, Lovisolo C, Siefritz F, Kaldenhoff R. The tobacco aquaporin NtAQP1 is a membrane CO_2 pore with physiological functions. Nature. 2003; 425:734–737. [PubMed: 14520414]
29. Nakhoul N, Davis B, Romero M, Boron W. Effect of expressing the water channel aquaporin-1 on the CO_2 permeability of *Xenopus* oocytes. Am J Physiol. 1998; 274:C543–C548. [PubMed: 9486145]
30. Cooper G, Boron W. Effect of PCMBS on CO_2 permeability of *Xenopus* Oocytes expressing aquaporin 1 or its C189S mutant. Am J Physiol. 1998; 275:C1481–C1486. [PubMed: 9843709]
31. Prasad GVT, Coury L, Finn F, Zeidel M. Reconstituted aquaporin 1 water channels transport CO_2 across membranes. J Biol Chem. 1998; 273:33123–33126. [PubMed: 9837877]
32. Cooper G, Zhou Y, Bouyer P, Grichtchenko I, Boron W. Transport of volatile solutes through AQP1. J Physiol. 2002; 542:17–29. [PubMed: 12096045]
33. Terashima I, Ono K. Effects of $HgCl_2$ on CO_2 dependence of leaf photosynthesis: Evidence indicating involvement of aquaporins in CO_2 diffusion across the plasma membrane. Plant Cell Physiol. 2002; 43:70–78. [PubMed: 11828024]
34. Blank M, Ehmke H. Aquaporin-1 and HCO_3^--Cl^- transporter-mediated transport of CO_2 across the human erythrocyte membrane. J Physiol. 2003; 550:419–429. [PubMed: 12754312]
35. Hanba YT, et al. Overexpression of the barley aquaporin HvPIP2;1 increases internal CO_2 conductance and CO_2 assimilation in the leaves of transgenic rice plants. Plant Cell Physiol. 2004; 45:521–529. [PubMed: 15169933]

36. Endeward V, et al. Evidence that Aquaporin 1 is a major pathway for CO_2 transport across the human erythrocyte membrane. FASEB J. 2006; 20:1974–1981. [PubMed: 17012249]
37. Herrera M, Hong NJ, Garvin JL. Aquaporin-1 transports NO across cell membranes. Hypertension. 2006; 48:157–164. [PubMed: 16682607]
38. Uehlein N, et al. Function of nicotiana tabacum aquaporins as chloroplast gas pores challenges the concept of membrane CO_2 permeability. Plant Cell. 2008; 20:648–657. [PubMed: 18349152]
39. Missner A, et al. Carbon dioxide transport through membranes. J Biol Chem. 2008; 283:25340–25347. [PubMed: 18617525]
40. Herrera M, Garvin J. Novel role of AQP-1 in no-dependent vasorelaxation. Am J Physiol Renal Physiol. 2007; 292:F1443–F1451. [PubMed: 17229677]
41. Yang B, et al. Carbon dioxide permeability of aquaporin-1 measured in erythrocytes and lung of aquaporin-1 null mice and in reconstituted proteoliposomes. J Biol Chem. 2000; 275:2682–2692.
42. Fang X, Yang B, Matthay M, Verkman A. Evidence against aquaporin-1-dependent CO_2 permeability in lung and kidney. J Physiol. 2002; 542:63–69. [PubMed: 12096051]
43. Verkman A. Does aquaporin-1 pass gas? An opposing view. J Physiol. 2002; 542:31. [PubMed: 12096046]
44. Wang Y, Cohen J, Boron WF, Schulten K, Tajkhorshid E. Exploring gas permeability of cellular membranes and membrane channels with molecular dynamics. J Struct Biol. 2007; 157:534–544. [PubMed: 17306562]
45. Hub JS, de Groot BL. Does CO_2 permeate through Aquaporin-1? Biophys J. 2006; 91:842–848. [PubMed: 16698771]
46. Amiry-Moghaddam M, et al. An alpha-syntrophin-dependent pool of aqp4 in astroglial end-feet confers bidirectional water flow between blood and brain. Proc Natl Acad Sci USA. 2003; 100:2106–2111. [PubMed: 12578959]
47. Sulyok E, Vajda Z, Dóczi T, Nielsen S. Aquaporins and the central nervous system. Acta Neurochir (Wien). 2004; 146:955–960. [PubMed: 15340804]
48. Manley GT, Binder DK, Papadopoulos MC, Verkman AS. New insights into water transport and edema in the central nervous system from phenotype analysis of aquaporin-4 null mice. Neuroscience. 2004; 129:983–991. [PubMed: 15561413]
49. Verkman A. More than just water channels: unexpected cellular roles of aquaporins. J Chem Soc. 2005; 118:3225–3232.
50. Rash J, Davidson K, Yasumura T, Furman C. Freeze-fracture and immunogold analysis of aquaporin-4 (AQP4) square arrays, with models of AQP4 lattice assembly. Neuroscience. 2004; 129:915–934. [PubMed: 15561408]
51. Rash J, Yasumura T, Hudson C, Agre P, Nielsen S. Direct immunogold labeling of aquaporin-4 in square arrays of astrocyte and ependymocyte plasma membranes in rat brain and spinal cord. Proc Natl Acad Sci USA. 1998; 95:11981–11986. [PubMed: 9751776]
52. Suzuki H, Nishikawa K, Hiroaki Y, Fujiyoshi Y. Formation of aquaporin-4 arrays is inhibited by palmitoylation of n-terminal cysteine residues. Biochim Biophys Acta. 2008; 1778:1181–1189. [PubMed: 18179769]
53. Ignarro LJ. Nitric oxide: a unique endogenous signaling molecule in vascular biology. Biosci Rep. 1999; 19:51–71. [PubMed: 10888468]
54. Ignarro LJ. Nitric oxide as a unique signaling molecule in the vascular system: a historical overview. J Physiol Pharmacol. 2002; 53:503–514. [PubMed: 12512688]
55. Murad F. Discovery of some of the biological effects of nitric oxide and its role in cell signaling. Biosci Rep. 2004; 24:452–474. [PubMed: 16134022]
56. Pacher P, Beckman J, Liaudet L. Nitric oxide and peroxynitrite in health and disease. Physiol Rev. 2007; 87:315–424. [PubMed: 17237348]
57. Wang, Y.; Ohkubo, YZ.; Tajkhorshid, E. Gas conduction of lipid bilayers and membrane channels. chapter 12. In: Feller, S., editor. Current Topics in Membranes: Computational Modeling of Membrane Bilayers. Elsevier; 2008. p. 343-367.
58. Humphrey W, Dalke A, Schulten K. VMD – Visual Molecular Dynamics. J Mol Graphics. 1996; 14:33–38.

59. Cohen J, Kim K, King P, Seibert M, Schulten K. Finding gas diffusion pathways in proteins: Application to O_2 and H_2 transport in CpI [FeFe]-hydrogenase and the role of packing defects. Structure. 2005; 13:1321–1329. [PubMed: 16154089]
60. Cohen J, Arkhipov A, Braun R, Schulten K. Imaging the migration pathways for O_2, CO, NO, and Xe inside myoglobin. Biophys J. 2006; 91:1844–1857. [PubMed: 16751246]
61. Roux B. The calculation of the potential of mean force using computer simulations. Computer Physics Communications. 1995; 91:275–282.
62. Phillips JC, et al. Scalable molecular dynamics with NAMD. J Comp Chem. 2005; 26:1781–1802. [PubMed: 16222654]
63. MacKerell A Jr, Bashford D, Bellott M, et al. All-atom empirical potential for molecular modeling and dynamics studies of proteins. J Phys Chem B. 1998; 102:3586–3616.
64. Feller SE, Zhang YH, Pastor RW, Brooks BR. Constant pressure molecular dynamics simulation — the Langevin piston method. J Chem Phys. 1995; 103:4613–4621.
65. Darden T, York D, Pedersen L. Particle mesh Ewald. An N·log(N) method for Ewald sums in large systems. J Chem Phys. 1993; 98:10089–10092.
66. de Groot BL, Frigato T, Helms V, Grubmüller H. The mechanism of proton exclusion in the aquaporin-1 water channel. J Mol Biol. 2003; 333:279–293. [PubMed: 14529616]
67. Zhu F, Tajkhorshid E, Schulten K. Molecular dynamics study of aquaporin-1 water channel in a lipid bilayer. FEBS Lett. 2001; 504:212–218. [PubMed: 11532456]
68. Hub J, de Groot B. Mechanism of selectivity in aquaporins and aquaglyceroporins. Proc Natl Acad Sci USA. 2008; 105:1198–1203. [PubMed: 18202181]
69. Hiroaki Y, et al. Implications of the aquaporin-4 structure on array formation and cell adhesion. J Mol Biol. 2006; 355:628–639. [PubMed: 16325200]
70. Garthwaite J. Concepts of neural nitric oxide-mediated transmission. Eur J Neurosci. 2008; 27:2783–2802. [PubMed: 18588525]
71. Lin L, Taktakishvili O, Talman W. Identification and localization of cell types that express endothelial and neuronal nitric oxide synthase in the rat nucleus tractus solitarii. Brain Res. 2007; 1171:42–51. [PubMed: 17761150]
72. Smart O, Goodfellow J, Wallace B. The pore dimensions of Gramicidin A. Biophys J. 1993; 65:2455–2460. [PubMed: 7508762]

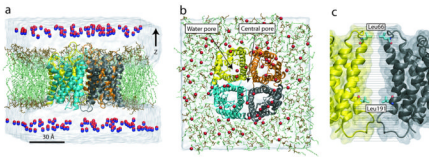

Figure 1.

Simulation systems. Side view (a) and top view (b) of the explicit gas diffusion simulation system. The AQP4 tetramer is embedded in a lipid bilayer (head group: brown, tail: green), with the four monomers colored in yellow, orange, cyan, and black, respectively. 150 NO molecules are placed in the bulk water, ~10 Å away from the membrane. Water is shown as a transparent box. (c) Close-up view of the umbrella sampling simulation system. The central pore is divided into 33 windows, with the center of each window represented by a black line. While most windows are placed ~1 Å apart, more are added near the two entrances of the central pore (Leu66 and Leu191) to improve sampling in these narrow regions.

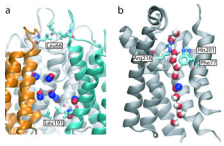

Figure 2.
Explicit gas diffusion simulation results. (a) Seven NO molecules entered the central pore of AQP4 spontaneously in the 50-ns explicit gas diffusion simulation. (b) NO molecules also entered the water pore spontaneously. However, no NO molecule is observed in the selectivity filter (Arg216, Phe77 and His201), which is the narrowest region of the water pore.

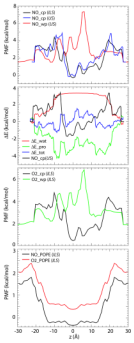

Figure 3.

PMF of NO and O_2 permeation through AQP4 and a POPE bilayer. (a) PMF of NO permeation through AQP4 central pore (NO_{-cp}) and water pores (NO_{-wp}), calculated using both umbrella sampling (*US*) and implicit ligand sampling (*ILS*). (b) Enthalpic contributions (ΔE_{tot}) to the PMF of NO permeation ($NO_{-cp}(US)$), calculated from interaction energy of NO with protein (ΔE_{pro}), and with water (ΔE_{wat}). (c) PMF of O_2 permeation through AQP4. (d) PMF of NO and O_2 permeation through a POPE bilayer. In all PMFs, $z = 0$ is set to the center-of-mass of the AQP4 tetramer or the center of the bilayer. The reference point of all PMFs is vacuum, except for (b) (see Methods).

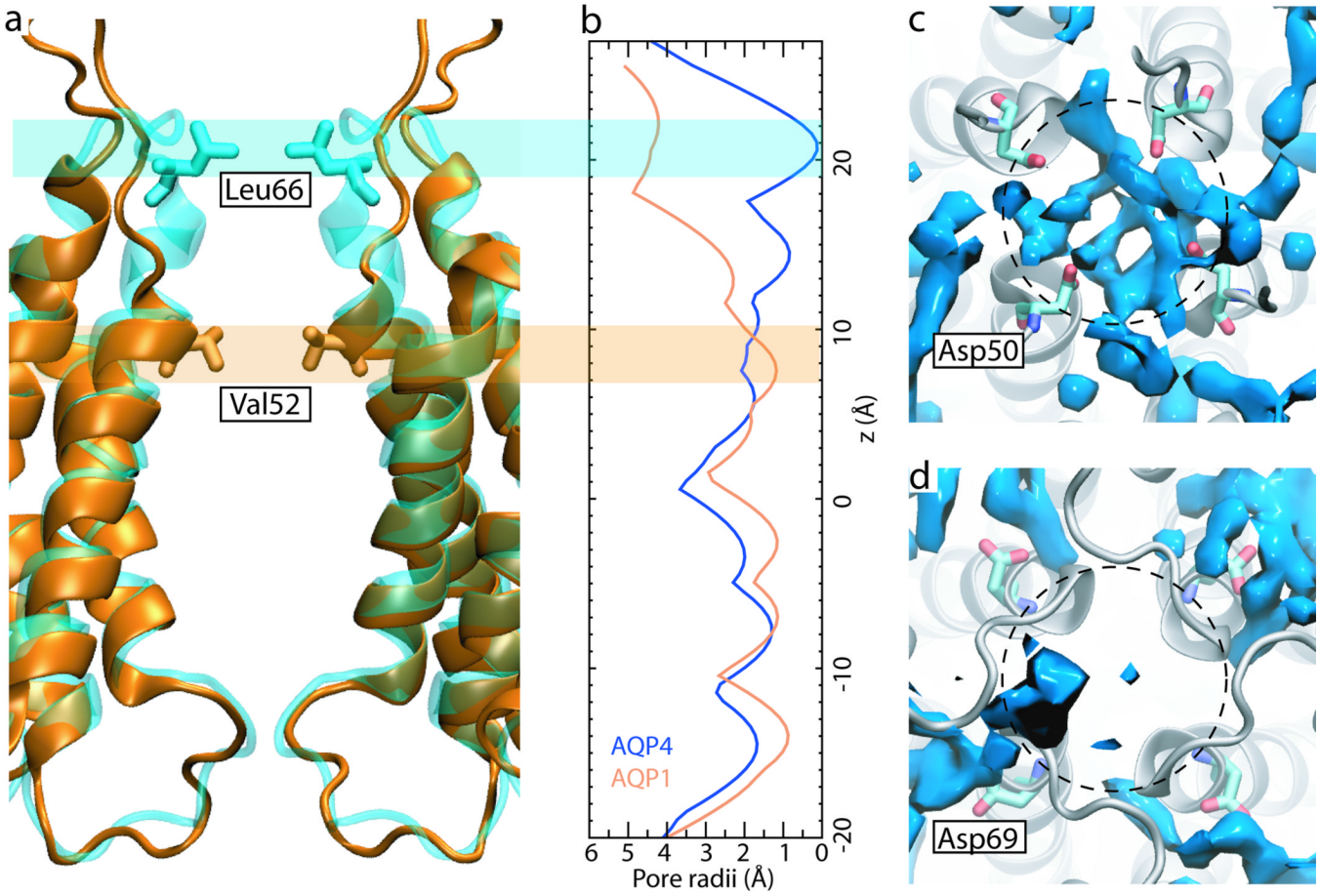

Figure 4.

Comparison of AQP4 and AQP1 central pores. (a) Superposition of AQP4 (blue) and AQP1 (orange). The transmembrane helix H2 in AQP4 extends an extra turn, making the central pore ~10 Å longer than that of AQP1. (b) Radii of AQP4 and AQP1 central pores calculated based on their crystal structures using the program HOLE (72). Residues Leu66 in AQP4 and Val52 in AQP1 correspond to the narrowest part in the periplasmic entrance of the two central pores. (c,d) The water occupancy in the periplasmic entrance of the AQP1 (c) and AQP4 (d) central pores. Shown in blue is the volume occupied by water during ≥75% time of the respective simulation. Approximate positions of the central pores are shown using dashed circles. Residues Asp69 in AQP4 relocate the high density water layer to the periphery of the central pore, leaving its entrance “clear”.

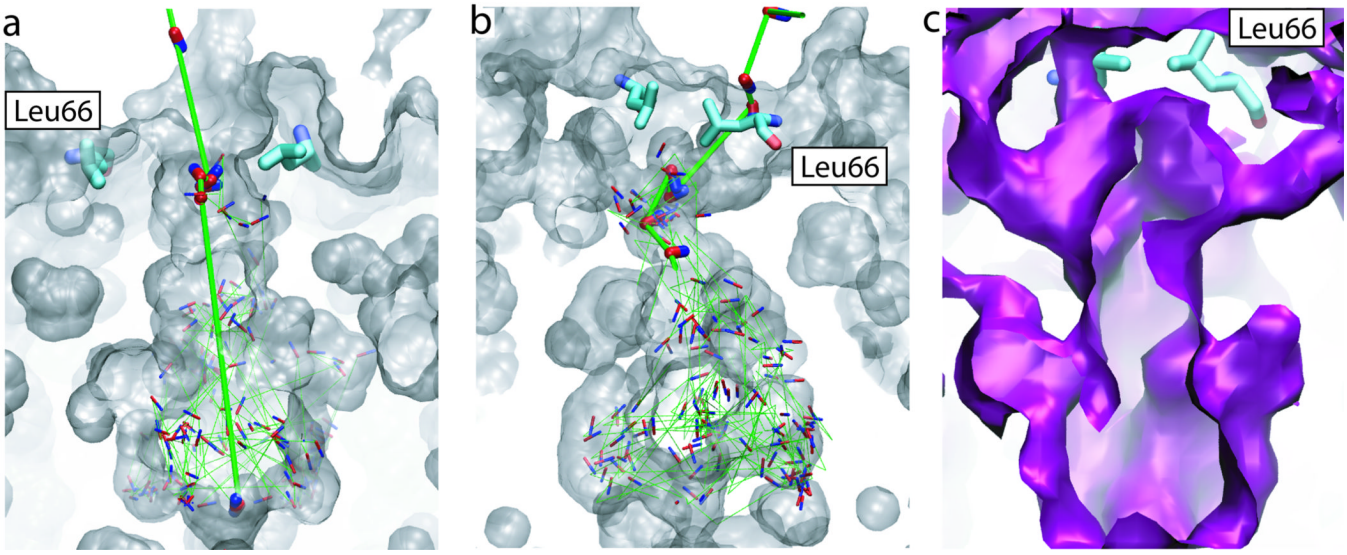

Figure 5.
Multiple pathways for gas permeation through the central pore. (a) and (b) Two representative pathways revealed by the explicit gas diffusion simulation. The central pore is shown in transparent gray surface. Snapshots of a NO molecule taken every 50–150 ps are shown in red and blue sticks, with its trajectory shown using green lines. To highlight the entry of NO into the central pore, gas molecules from the first few snapshots are drawn using thick sticks, with their trajectories shown in thick green lines. (c) The existence of multiple pathways revealed by implicit ligand sampling. The 2 kcal/mol energy isosurface of the 3D PMF is shown in purple.